Earth Syst. Sci. Data, 16, 5009–5026, 2024
https://doi.org/10.5194/essd-16-5009-2024

Open Access Earth System Science Data

An integrated dataset of ground hydrothermal regimes and soil nutrients monitored in some previously burned areas in hemiboreal forests in Northeast China during 2016–2022

Xiaoying Li[1], Huijun Jin[1,2,3], Qi Feng[4], Qingbai Wu[1], Hongwei Wang[1,2], Ruixia He[1], Dongliang Luo[1], Xiaoli Chang[1,5], Raul-David Şerban[6], and Tao Zhan[3]

[1]Key Laboratory of Cryospheric Science and Frozen Soil Engineering, Northwest Institute of Eco-Environment and Resources, Chinese Academy of Sciences, Lanzhou 730000, China
[2]School of Ecology, Northeast Forestry University, Harbin 150040, China
[3]Ministry of Natural Resources Field Observation and Research Station of Permafrost and Cold Regions Environment in the Da Xing'anling Mountains at Mo'he, Natural Resources Survey Institute of Heilongjiang Province, Harbin 150036, China
[4]Key Laboratory of Ecohydrology of Inland River Basin, Northwest Institute of Eco-Environment and Resources, Chinese Academy of Sciences, Lanzhou 730000, China
[5]School of Earth Sciences and Spatial Information Engineering, Hunan University of Science and Technology, Xiangtan, Hunan 411202, China
[6]Faculty of Agricultural, Environmental and Food Sciences, Free University of Bozen-Bolzano, 39100 Bolzano, Italy

Correspondence: Huijun Jin (hjjin@nefu.edu.cn)

Received: 15 May 2024 – Discussion started: 3 June 2024
Revised: 23 August 2024 – Accepted: 9 September 2024 – Published: 30 October 2024

Abstract. Under a warming climate, the occurrence of wildfires has been becoming increasingly more frequent in boreal forests and Arctic tundra over the last few decades. Wildfires can cause radical changes in forest ecosystems and the permafrost environment, such as the irreversible degradation of permafrost, succession of boreal forests, rapid and massive losses of soil carbon stock, and increased periglacial geohazards. Since 2016, we have gradually and more systematically established a network for studying soil nutrients and monitoring the hydrothermal state of the active layer and near-surface permafrost in the northern Da Xing'anling Mountains in Northeast China. Soil moisture content (depth of 0–9.4 m), soil organic carbon content (0–3.6 m), total nitrogen content (0–3.6 m), and total phosphorus and potassium content (0–3.6 m) datasets were obtained in 2016 via field sampling and subsequent laboratory tests. Ground temperature (0–20 m) and active layer thickness (2017–2022) datasets were obtained using thermistor cables that were permanently installed in boreholes or interpolated with these temperatures. The present data can be used to simulate changes in permafrost features under a changing climate and wildfire disturbances and to explore the changing interactive mechanisms of the fire–permafrost–carbon system in hemiboreal forests. Furthermore, they can provide baseline data for studies and action plans to support the carbon neutralization initiative and assessment of the ecological safety and management of the permafrost environment. These datasets can be easily accessed via the National Tibetan Plateau/Third Pole Environment Data Center (https://doi.org/10.11888/Cryos.tpdc.300933, Li and Jin, 2024).

Published by Copernicus Publications.

1 Introduction

As a key component of the Northern Hemisphere, permafrost and its changes can have substantial consequences for natural and anthropogenic systems (Smith et al., 2022). Moreover, due to its high sensitivity to climate warming, surface disturbances, and human activities, permafrost has undergone extensive degradation during the last 6 decades (e.g., Biskaborn et al., 2019; Chang et al., 2024; Jin et al., 2000, 2007, 2021, 2022, 2023; G. Li et al., 2022; Petrov et al., 2022). As one of the most common natural agents and disturbance factors in boreal forests, wildfires can initiate ecosystem renewal at different spatiotemporal scales (Johnstone et al., 2004; Li et al., 2019). Wildfires initially impact the permafrost environment by modifying or altering the ground hydrothermal regimes (Jorgenson et al., 2013; X. Li et al., 2022a; Yoshikawa et al., 2003); they can then subsequently induce modifications or radical/irreversible changes in biogeochemical processes (e.g., Fultz et al., 2016; Li et al., 2023; Ping et al., 2010; Xu et al., 2024). In boreal forests, wildfires have become increasingly more frequent in recent decades under a warming climate and due to increasing human activity in these areas (Boyd et al., 2023; Chen et al., 2023; Knorr et al., 2016; Westerling et al., 2006). Moreover, the region immediately south of the Arctic circle (50–67° N) experienced a greater number of vegetation fires compared with the Arctic (north of 67° N) in 2001–2020 (Chen et al., 2023). Although the total burned area on Earth may be declining, the fire behavior was worsening in several regions in 2003–2023, particularly in the boreal and temperate conifer biome (Cunningham et al., 2024).

In boreal regions, vegetation and the soil organic layer are essential buffering and protective layers with respect to the underlying permafrost. The combustion of all vegetation cover and the partial or complete removal of the insulating organic layer have direct hydrothermal impacts on permafrost: this reduces the land surface albedo, increases the ground surface and cryosol/ice exposure to direct solar radiation, and weakens the cooling effects of vegetative shading and evapotranspiration (Johnstone et al., 2010; Nossov et al., 2013; Shur and Jorgenson, 2007; Yoshikawa et al., 2003). All of these factors contribute to a higher ground surface temperature and more heat being transferred into the ground, resulting in rapid ground warming and a sharp deepening of the active layer (X. Li et al., 2022a; Michaelides et al., 2019; Nossov et al., 2013; Smith et al., 2015). In Interior Alaska, the organic layer thickness decreased from 21 to 4 cm after fire, resulting in the thaw depth increasing from 72 to 152 cm, the mean annual surface temperature rising from −0.6 to +2.1 °C, and the mean annual deep temperature increasing from −1.7 to +0.4 °C (Nossov et al., 2013). In the boreal zone, 6–11 years after fire, the mean annual ground temperature (MAGT) increased by 1.5–2.3 °C (Li et al., 2021; Munkhjargal et al., 2020; Nossov et al., 2013; Smith et al., 2015); moreover, even the mean annual ground surface temperature in burned areas was still 2–3 °C higher than those in unburned areas 80 years after fire (Brown et al., 2015). Meanwhile, 25 years after a fire, the active layer thickness (ALT) was found to have increased by 2.75 m, from an initial value of 45 cm, and it had not recovered to the pre-fire level 36 years after the fire (Viereck et al., 2008). In central Siberia, it generally takes 70–80 years for the active layer to return to its pre-fire state (Kirdyanov et al., 2020). Forest fires can also cause significant changes in the soil moisture content, which in turn affects ground thermal regimes (Nossov et al., 2013). Due to the fire-induced thaw of permafrost, charred moss layers with lowered infiltration rates, lower transpiration rates, and reduced evapotranspiration in severely burned areas, surface soil moisture contents (generally less than a depth of 30 cm) at burned sites were significantly higher than those at unburned sites (Kopp et al., 2014; Potter and Hugny, 2020; Yoshikawa et al., 2003). However, affected by soil texture, permafrost thaw after a fire can also lead to a decrease in the soil moisture content (X. Li et al., 2022a; Nossov et al., 2013). In summary, in the short term, forest fires decrease transpiration rates and increase soil moisture; however, in the long-term (more than a decade), an increased ALT and the recovery of vegetation reduce the soil moisture content at burned sites compared with those at unburned sites (Yoshikawa et al., 2003). Moreover, changes in ground hydrothermal regimes and the ALT would decline and progressively dwindle with ecosystem recovery and organic layer regrowth over time under a stable or cooling climate (e.g., Holloway et al., 2020; Rocha et al., 2012).

Arctic boreal permafrost soils contain between 1100 and 1500 Pg ($1\,\mathrm{Pg} = 10^{15}$ g) carbon, approximately twice the amount of the atmospheric carbon pool (Hugelius et al., 2014), and account for nearly half the global belowground organic carbon pool (O'Donnell et al., 2011a). Wildfire disturbances have important and long-term ramifications for terrestrial carbon cycling and carbon stocks (Chen et al., 2022; Dieleman et al., 2022; Genet et al., 2013; O'Donnell et al., 2011a, b). Unlike gradual thawing, abrupt changes in ground hydrothermal regimes after fires often disrupt the entire soil profile and initiate or aggravate carbon loss from deep permafrost soils (Jones et al., 2015; Turetsky et al., 2019). Therefore, the combustion of vegetation and the subsequent thaw of permafrost have resulted in rapid releases of large amounts of carbon and nitrogen into the atmosphere as greenhouse gases (Mack et al., 2011, 2021; Taş et al., 2014). Furthermore, over a short time, abrupt permafrost thaw would possibly result in the emission of more methane than gradual thaw (Koven et al., 2015). Therefore, in the boreal permafrost region, wildfires exacerbate the rates of permafrost thaw and alter soil organic carbon dynamics in both organic and mineral soils. In addition to soil organic carbon, forest fires potentially also reduce the soil nitrogen content, inducing shifts in nutrient cycling in the boreal forest and permafrost regions (Certini, 2005; Knicker, 2007; Kolka et al., 2017). However, there are inconsistent reports regarding

the effects of forest fire on soil phosphorus and potassium. Some studies show a significant post-fire reduction in phosphorus and potassium, while other studies indicate an evident increase after light burns or a reduction after severe burns as well as nearly unchanged stocks of potassium and phosphorus (Gu et al., 2010; Neff et al., 2005; Zhao et al., 1994). As a result, wildfires in boreal permafrost regions had been considered to trigger strong positive feedbacks on climate warming via massive emissions of biogenic major greenhouse gases (Koven et al., 2015; Ramm et al., 2023).

Located on the southern margin of the eastern Asian boreal forests and permafrost regions, the Da Xing'anling Mountains in Northeast China are prone to frequent and massive wildfires. The Xing'an permafrost in this area is controlled or strongly affected by many local factors, such as dense vegetation cover, a thick organic layer, stable snow cover, and anthropic development (Jin et al., 2007; Şerban et al., 2021; Wang et al., 2024). The warm and thin permafrost in the Da Xing'anling Mountains in Northeast China is located in the discontinuous permafrost zone. Therefore, this ecosystem-dominated (ecosystem-driven, -modified, or -protected) permafrost is sensitive to climate warming and wildfires (Shur and Jorgenson, 2007). Compared with the Arctic permafrost region, the permafrost monitoring network in this area has been established quite recently; thus, readily accessible and shared permafrost data from this network are currently inadequate. Similarly, permafrost monitoring data from burned areas in the boreal permafrost region in China are meagre in comparison with those from other northern countries or regions, but they are increasing. Prior to the early 1980s, there was little research on wildfire impacts on the permafrost environment in Northeast China. In the early 1990s, there were a few occasional fire-related geocryological studies and limited site-specific measurements of soil temperature and moisture content in the active layer and near-surface (depth of ≤ 20 m) permafrost near the town of Amu'er in northern Heilongjiang Province (Liang et al., 1991; Zhou et al., 1993). However, research on fire impacts on soil carbon and nitrogen pools and cycles in the Xing'an permafrost in Northeast China has just started and is still in its infancy. Due to the cold and arid climate in winter and spring, complex mountain topography, and dense hemiboreal vegetation in the region, fire regimes are often complex. In addition, burned areas are often located in pristine forest areas far away from roads, making it challenging to readily access and study fire impacts. Therefore, it is difficult to systematically understand and quantitatively evaluate the effects of wildfires on ground hydrothermal regimes and carbon stocks at different spatiotemporal scales (Li et al., 2021).

To address the abovementioned issues, an observation system has gradually been established in the northern Da Xing'anling Mountains since 2016, with the aim of studying the area's ground hydrothermal regimes and soil nutrient content. The dataset from this network can provide important auxiliary data for studying permafrost landscapes, carbon stocks, and boreal ecology and hydrology. It can also provide important information for the management of land and water resources and the ecological environment after wildfire disturbances in Northeast China, particularly in forested hemiboreal permafrost regions. In Sect. 2 of this paper, we first introduce the comprehensive permafrost and soil nutrient observation network in the northern Da Xing'anling Mountains. The design of the ground hydrothermal regime and systematic soil nutrient content observation monitoring network and an evaluation of the data quality are given in Sect. 2. In Sect. 3, the permafrost hydrothermal regime and soil nutrient observations that provide a 6-year-long dataset are described and briefly interpreted, with a focus on major features of the observation network for a better understanding of the dataset structure and content. The data availability and accessibility are outlined in Sect. 4, and major conclusions and prospects for future work are given in Sect. 5. This dataset provides important input for model simulations of permafrost changes due to fire disturbances and a warming climate, especially the rapid and abrupt degradation of the Xing'an permafrost and resultant periglacial phenomena, such as thermokarst, thaw settlement, and ground surface subsidence and ponding. This is useful for analyzing the interactive hydrothermal and cyclic mechanisms of the wildfire–permafrost–carbon system in hemiboreal forests.

2 Monitoring networks and data processing

2.1 Study area descriptions and monitoring networks

A permafrost monitoring network has been established in four burned areas in the northern Da Xing'anling Mountains in Northeast China in boreal forest and discontinuous permafrost regions (Fig. 1). Two of these areas are located in shrub wetlands in Mo'he (MH) city and Gulian (GL) town in northern Heilongjiang Province. The other two areas are located in larch forests in Alongshan (AL) and Mangui (MG) towns in the northeastern part of Inner Mongolia. The network includes eight sites in the four burned areas with two fire severity levels (severely burned, S, and unburned, U) from 1987 to 2015 (the fire severity division method is shown in Sect. 2.2). The studied forest fire in MH (which resulted in severely burned, MH-S, and unburned, MH-U, sites) occurred on 6 May 1987 and induced a burned area of 1.01×10^6 ha; that in GL (which resulted in severely burned, GL-S, and unburned, GL-U, sites) occurred on 28 July 2002 and induced a burned area of 1121 ha; that in AL (which resulted in severely burned, AL-S, and unburned, AL-U sites) occurred on 10 May 2009 and induced a burned area of 930 ha; and that in MG (which resulted in severely burned, MG-S, and unburned, MG-U, sites) occurred on 12 July 2015 and induced a burned area of 237 ha.

The study areas are characterized by a cold temperate continental climate. In the study areas of GL and MH, based on data from the nearby Mo'he weather station from 1960 to

2020, the mean annual air temperature (MAAT) ranged from −6.2 to −2.4 °C, with an average rate of climate warming of 0.3 °C per decade; annual precipitation was 274–675 mm, with a slight average wetting trend of 13.8 mm per decade. In the study areas of MG and AL, based on data from the nearby Huzhong weather station from 1974 to 2020, the MAAT varied from −5.2 to −2.0 °C, with the same climate warming rate as that of Mo'he (0.3 °C per decade); annual precipitation was 272–749 mm, showing an appreciable average wetting rate of 3.1 mm per decade. Precipitation fell concentratively in the form of rain from June to August, accounting for 62 %–65 % of the annual total. Snow cover generally lasted from October to the following May, with maximum snow depths of 40–50 cm.

The four study areas were selected to observe post-fire changes in permafrost features and soil nutrient conditions (Table 1). This monitoring network includes eight boreholes and soil profiles and major elements of the observational network for ground temperature, ALT, soil moisture content (SMC), soil organic carbon (SOC), total nitrogen (TN), total phosphorus (TP), and total potassium (TK). The MAGT at the depth of zero annual amplitude (D_{ZAA}, generally at a depth of 10–15 m) ranged from −3.25 to −0.56 °C, and measured ALT varied from 1.0 to 3.75 m. The four study areas were all found in the zones of discontinuous permafrost, with poor drainage in lowlands and intermontane basins or valleys. The soils in the study area are mainly Histosols and Gelisols (Soil Survey Staff, 2014). Before fires, vegetation was dominated by Xing'an larch (*Larix gmelinii*) forest, generally with an understory mainly consisting of *Ledum palustre* and *Vaccinium uliginosum* shrubs, with an organic layer of 55–60 cm thickness. After fires, the vegetation of the burned areas became gradually dominated by white birch (*Betula platyphylla*) and dwarf bog birch (*Betula fruticosa* Pallas), with an organic layer of 20–30 cm thickness. At severely burned sites in AL, GL, and MH, measurements of the organic-matter thickness were taken 7, 14, and 29 years after fires, so it was possible that the organic layer thickness exceeded 20 cm due to the re-accumulation of organic matter. At the severely burned site in MG, the organic-matter residue after combustion was in a fluffy state with a thickness of 20 cm. When the re-accumulation or residual organic matter exceeded 20 cm, the rates of active layer thickening and soil temperature increase after fires were slowed, and the permafrost gradually recovered with the re-accumulation of the organic layer.

The horizontal distance between the MG-U and MG-S sites was about 200 m, with the MG-U site being located on the edge of the burned area. Observations of ground temperature began in February 2017 (2 years after fire). At MG-U, the vegetation comprised Xing'an-larch-dominated (*Larix gmelinii*-dominated) forest, whereas all larch trees at MG-S were burned to death, and only low shrubs and herbs were found in 2022. The horizontal distance between AL-U and AL-S was less than 100 m, with the AL-U site being located on the edge of the burned area. Observations of ground temperature began in February 2017 (8 years after fire). The vegetation at AL-U was Xing'an larch forest, whereas it was broad-leaved forest (birch) at AL-S. The horizontal distance between the GL-S and GL-U sites was about 2 km. Measurements of ground temperature began in February 2017 (15 years after fire). The vegetation at GL-U and GL-S was shrub wetland. The MH-S and MH-U sites were about 5 km apart. Observations of ground temperature began in February 2017 (30 years after fire). The ecosystem at MH-U and MH-S was characteristic of shrub wetlands.

2.2 Fire severity

The normalized burn ratio (NBR) and differential normalized burn ratio (dNBR) are often used to assess forest fire severity (Cocke et al., 2005; X. Li et al., 2022a). The calculation formulas for these metrics are as follows:

$$\mathrm{NBR} = (\rho_{\mathrm{NIR}} - \rho_{\mathrm{MIR}})/(\rho_{\mathrm{NIR}} + \rho_{\mathrm{MIR}}), \quad (1)$$

$$\mathrm{dNBR} = \mathrm{NBR}_{\mathrm{prefire}} - \mathrm{NBR}_{\mathrm{postfire}}, \quad (2)$$

where ρ_{NIR} and ρ_{MIR} are the reflectivity values of pixels from the near-infrared (NIR) and middle-infrared (MIR) bands, respectively, and $\mathrm{NBR}_{\mathrm{prefire}}$ and $\mathrm{NBR}_{\mathrm{postfire}}$ are the values of NBR before and after fire, respectively.

According to Cocke et al. (2005) and Roy et al. (2006), dNBR values of 0.241 and 0.57 are critical values for the division between lightly and moderately burned areas and between moderately and severely burned areas. Therefore, via the vegetation burn status and comparison with dNBR values (Key and Benson, 2006; Escuin et al., 2008), fire severity is divided into four categories: severely burned ($\mathrm{dNBR} \geq 0.571$), moderately burned (0.241–0.570), lightly burned (0.051–0.240), and unburned (≤ 0.050) (Cocke et al., 2005). In the lightly and moderately burned areas, there were difficulties with respect to drilling and/or monitoring due to device malfunction or damage. In addition, the permafrost environment changes more significantly after severe burns. Therefore, only sites of two levels of fire severity (severely burned and unburned) were chosen in the abovementioned four areas (Mangui, MG; Alongshan, AL; Gulian, GL; and Mo'he, MH) to study post-fire changes in the ground hydrothermal regimes and soil nutrients.

2.3 Site instrumentation and laboratory analysis

At each unburned and severely burned site, a 20 m deep borehole was drilled and instrumented in October 2016 to monitor ground temperatures (eight boreholes in total) (Fig. 2). Ground temperatures were monitored at 0.5 m depth intervals between depths of 0 and 5 m and at 1 m depth intervals between depths of 5 of 20 m, using thermistor cables permanently installed in boreholes and manually measured from February 2017. All thermistors were assembled and

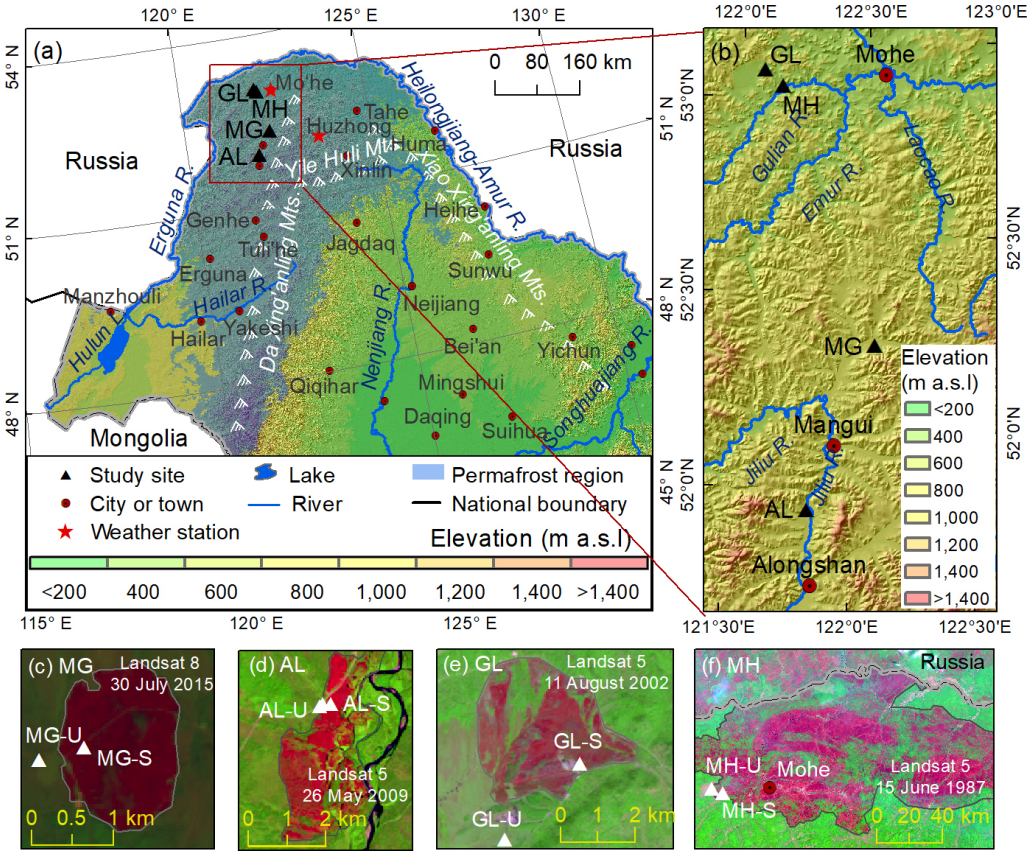

Figure 1. Location of the study areas and sites in the northern Da Xing'anling Mountains, Northeast China. The base map of the permafrost distribution is modified from X. Li et al. (2022b). The light-blue areas in panel **(a)** are the permafrost region. Panels **(c)** to **(f)** are false-color composite images of the remote sensing image; the burned areas are marked as pink, and the unburned areas are marked as green.

Table 1. Characteristics of the eight study sites for monitoring the thermal state and soil nutrients of the active layer and near-surface permafrost in the northern Da Xing'anling Mountains in Northeast China.

Study areas and sites		Latitude (° N)	Longitude (° E)	Elevation (m a.s.l.)	Vegetation	Organic layer thickness (cm)	Drainage	Fire severity
MG (Mangui)	MG-S	52.2765	122.2891	710	Larch forest	20	Somewhat poor	Severely burned
	MG-U					55	Poor	Unburned
AL (Alongshan)	AL-S	51.8868	121.9067	669	Larch forest	25	Moderately good	Severely burned
	AL-U					55	Poor	Unburned
GL (Gulian)	GL-S	53.0432	122.0504	582	Shrub wetland	30	Somewhat poor	Severely burned
	GL-U					60	Poor	Unburned
MH (Mo'he)	MH-S	52.9859	122.1115	486	Shrub wetland	30	Somewhat poor	Severely burned
	MH-U					60	Poor	Unburned

calibrated at the Key Laboratory of Cryospheric Science and Frozen Soil Engineering, Northwest Institute of Eco-Environment and Resources (renamed following the merger of the former State Key Laboratory of Frozen Soil Engineering and the State Key Laboratory of Cryosphere Science, Cold and Arid Regions Environmental and Engineering Research Institute), Chinese Academy of Sciences. Since February 2017, ground temperatures at these boreholes have been manually measured thrice monthly (Table 2) or, occasionally, once or twice monthly due to traffic difficulty or control, using a Fluke 189® multimeter device. According to the measured soil temperatures during the observation period, the isotherms of soil temperature in the vertical profile at depths of 0–20 m were drawn, and the 0 °C isotherms were then delineated for each borehole. Following this, the values of ALT were determined, using the linear extrapolation of the seasonally and progressively changing ground temperature distribution with depth, for each borehole and each year according to the deepest position of the 0 °C isotherms in the year.

While drilling in 2016, soil samples were collected from depths of 0–9.4 m at intervals of 0.1–3.0 m, resulting in a total of 402 soil samples. Three replicas were collected at the same depth, and the three samples were then evenly mixed into one. At depths of 0–3.0 m, samples were collected at depth increments of 10 cm in the soil strata, with more significant changes in soil organic matter and lithology near the ground surface. At depths of 3.0–9.4 m, samples were collected based on lithological similarity or changes in soil or rock strata, rather than at an equal depth interval of 0.1 m. Therefore, at depths between 0 and 3 m, there were generally a set of data at a regular depth interval of 10 cm, but the depth intervals of datasets varied substantially between depths of 3 and 10 m. One part of the soil samples was collected using a cutting ring, stored in a 100 cm^3 aluminum specimen box, and immediately weighed (soil wet weight). The samples were then transported to the laboratory and dried at 105 °C to obtain the soil dry weight. Finally, gravimetrically based SMC was calculated using the mass of the soil before and after drying. The other part of the soil samples was collected and stored in Ziploc bags, brought to the laboratory in a timely manner for air-drying, and then passed through a 2 mm sieve for chemical analysis. The SOC and TN contents were measured via potassium dichromate oxidation reduction and Kjeldahl nitrate boiling-fluid injection methods, respectively (Nelson et al., 1982). The TP and TK contents were determined via Mo–Sb colorimetry and flame photometry, respectively (Sun et al., 2011). These data are shown as the mean ± standard error (SE). Changes in ground temperature and soil chemical properties were analyzed using the space-for-time chronosequence approach (Mack et al., 2021).

2.4 Data quality check

The measurement accuracy of ground temperature data was ±0.05 °C in the range from −30 to +30 °C but ±0.1 °C in the range from −45 to −30 °C and +30 to +50 °C. From 2020 to 2022, due to the breakout and persistence of the COVID-19 pandemic, some data were not collected in a timely manner, affecting the sampling intervals. Ground temperature data were being collected manually thrice monthly from February 2017; however, after the outbreak of the COVID-19 pandemic, the data were recorded once or twice monthly. In addition, some data were missing because of damaged, broken, or destroyed probes, solar panel batteries, or data loggers. From 6 February 2017 to 22 November 2022, a total of 28 890 data records were collected. Of these data points, 178 NA (not available) data resulted from probe damage. Thus, 28 712 valid data were collected. All of the missing data were near the ground surface, at a soil depth of between 0 and 5 cm. At MG-U, AL-U, AL-S, GL-S, and MH-S, all data were available. Of the 178 NA data, 74 were at MG-S (from 17 September 2019 to 22 November 2022), 52 were at GL-U (from 20 July 2019 to 13 February 2022), and 52 were at MH-U (from 20 July 2019 to 13 February 2022). Soil temperature data from manually monitored boreholes were quality-controlled for each measurement. Some studies have also shown that this method of monitoring ground temperature using drilling and probes is one of the most accurate, reliable, and intuitive methods for long-term monitoring of permafrost data (Chang et al., 2022; G. Li et al., 2022; Li and Jin, 2024; Zhao et al., 2021). Before the analysis of soil nutrient data and SMC data, we conducted outlier tests to ensure the accuracy of the data. These tests showed that all of the datasets have no outliers and that the samples are representative. There were 840 soil nutrient data and 195 SMC data.

3 Data descriptions and evaluation

3.1 Changes in ground temperatures of near-surface permafrost

Ground temperatures at depths of 0–20 m in the active layer and near-surface permafrost showed remarkable seasonal dynamics (Figs. 3 and 4). The amplitudes of changes in ground temperature decreased exponentially with increasing depth. At depths of 0–1 m, changes in the MAGT at eight sites were 1.5–10.2 °C larger than those at 1–20 m (Fig. 3a–d).

The MAGT values decreased with increasing depth, and the temperature difference between depths of 0.5 and 20 m was 0.2–2.1 °C (Table 3). From 2017 to 2022, ground temperature fluctuated in a sinusoidal pattern at depths of 0.5 to 2.0 m, and this dynamic change gradually disappeared with increasing depth (Figs. 3a–g and 5a–g). At a depth of 5 m, ground temperature was subzero or perennially cryotic (Figs. 4d, k, 5d, and k). At eight sites, the ground tem-

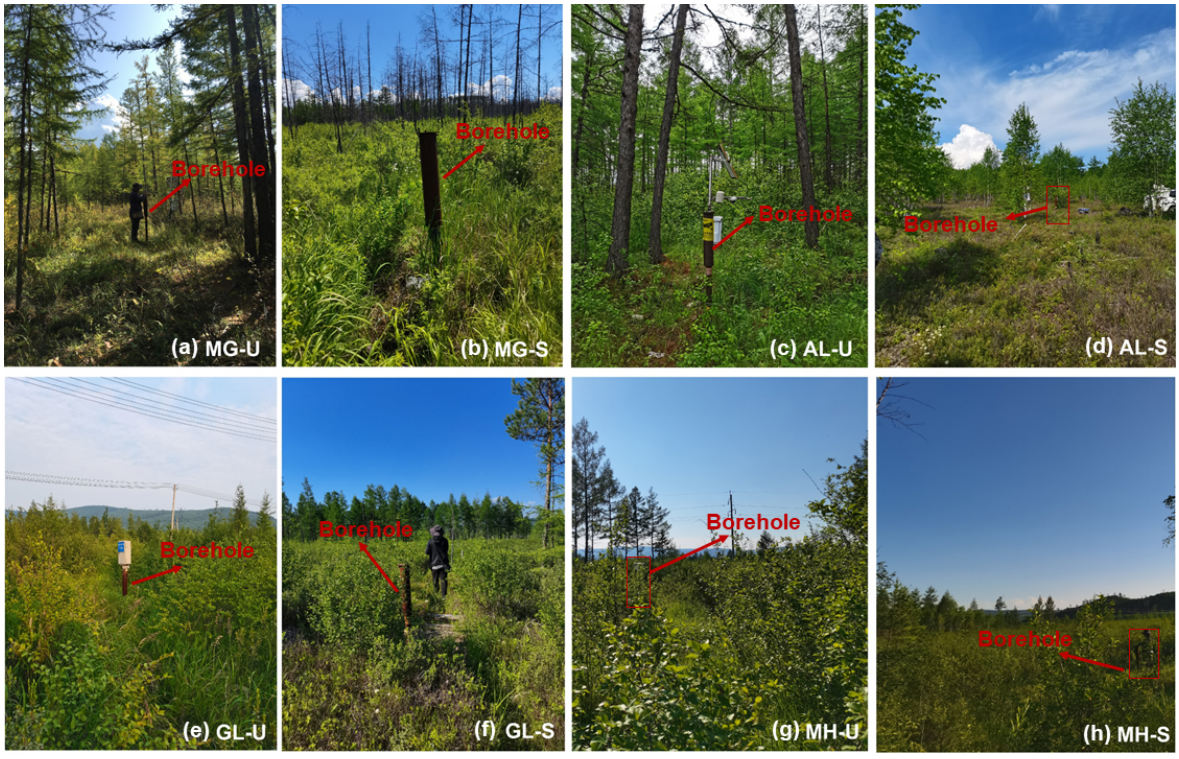

Figure 2. Photos of the study sites between 3 and 5 July 2022 showing the different vegetation cover and the position of the 20 m deep boreholes for monitoring the ground temperature in the northern Da Xing'anling Mountains in Northeast China. Panels **(a)** and **(b)** show the boreholes for the observation of ground temperature at severely burned and lightly burned Xing'an larch forest sites in MG; panels **(c)** and **(d)** show the boreholes for the observation of ground temperature at severely burned and lightly burned Xing'an larch forest sites in AL; panel **(e)** and **(f)** show the boreholes for the observation of ground temperature at severely burned and lightly burned shrub wetland sites in GL; and panels **(g)** and **(h)** show the boreholes for the observation of ground temperature at severely burned and lightly burned shrub wetland sites in MH.

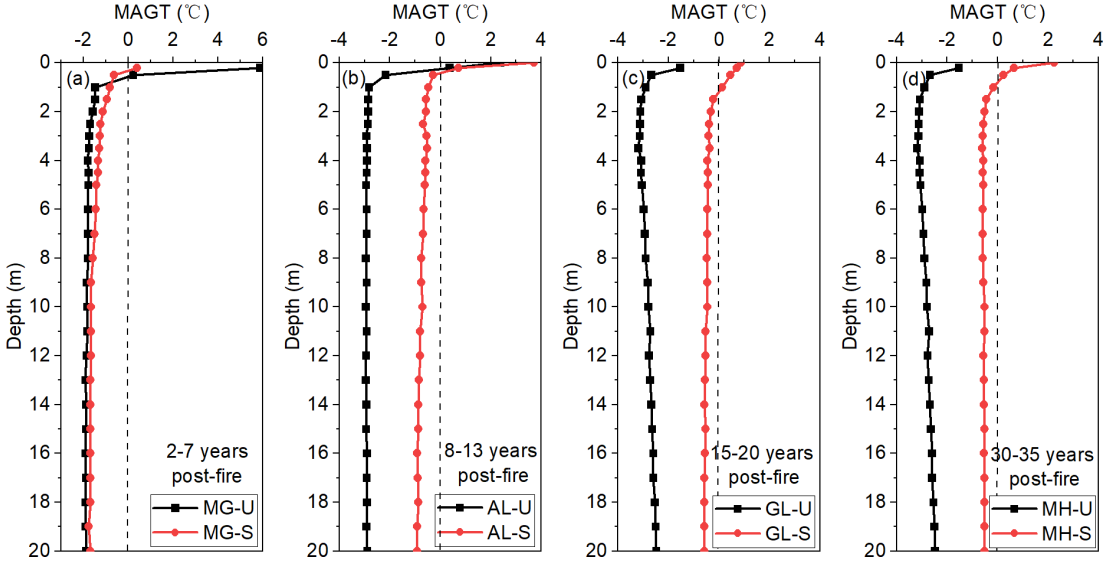

Figure 3. Mean annual ground temperatures (MAGTs) at the unburned and severely burned sites in the four areas on the western flank of the northern Da Xing'anling Mountains in Northeast China from 2017 to 2022.

Table 2. Soil nutrient and ground temperature borehole monitoring data from the eight sites for studying fire impacts on the permafrost environment in the northern Da Xing'anling Mountains in Northeast China.

Study sites	Monitoring depths (m)			Time period	Monitoring frequency
	Soil nutrients	Soil gravimetric moisture content (SMC)	Ground temperature		
MG-U	0.1, 0.2, 0.3, 0.4, 0.5, 0.6, 0.7, 0.8, 0.9, 1.0, 1.1, 1.2, 1.3, 1.4, 1.5, 1.6, 1.7, 1.8, 1.9, 2.0, 2.1, 2.2, 2.3, 2.4, 2.5	0.2, 0.3, 0.4, 0.5, 0.6, 0.7, 0.8, 0.9, 1.0, 1.1, 1.2, 1.3, 1.4, 1.5, 1.6, 1.7, 2.0, 2.5, 2.7	0.0, 0.2, 0.5, 1.0, 1.5, 2.0, 2.5, 3.0, 3.5, 4.0, 5.0, 6.0, 7.0, 8.0, 9.0, 10.0, 11, 12, 13, 14, 15, 16, 17, 18, 19, 20	2016; 2016; 2017–2022	Once; once; thrice per month
MG-S	0.1, 0.2, 0.3, 0.4, 0.5, 0.6, 0.7, 0.8, 0.9, 1.0, 1.1, 1.2, 1.3, 1.4, 1.5, 1.6, 1.7, 1.8, 1.9, 2.0, 2.1, 2.2, 2.3, 2.4, 2.5, 2.6	0.2, 0.3, 0.4, 0.5, 0.6, 0.7, 0.8, 0.9, 1.0, 1.1, 1.2, 1.3, 1.4, 1.5, 1.6, 1.7, 1.8, 1.9, 2.0, 2.1, 2.2, 2.6, 4.6, 5.6, 6.1, 7.6	0.0, 0.2, 0.5, 1.0, 1.5, 2.0, 2.5, 3.0, 3.5, 4.0, 5.0, 6.0, 7.0, 8.0, 9.0, 10.0, 11, 12, 13, 14, 15, 16, 17, 18, 19, 20	2016; 2016; 2017–2022	Once; once; thrice per month
AL-U	0.1, 0.2, 0.3, 0.4, 0.5, 0.6, 0.7, 0.8, 0.9, 1.0, 1.1, 1.2, 1.3, 1.4, 1.5, 1.6, 1.7, 1.8, 1.9, 2.0, 2.1, 2.2, 2.3, 2.4, 2.5, 2.6, 2.7, 2.8, 2.9, 3.0	0.1, 0.2, 0.3, 0.4, 0.5, 0.6, 0.7, 0.8, 0.9, 1.0, 1.1, 1.2, 1.3, 1.4, 1.5, 1.6, 1.7, 1.8, 1.9, 2.0, 2.1, 2.2, 2.3, 2.4, 2.5, 2.6, 2.7, 2.8, 2.9, 3.0, 3.1, 3.2, 3.5, 4.0, 4.5, 5.0, 5.5, 5.9, 6.4, 9.4	0.0, 0.2, 0.5, 1.0, 1.5, 2.0, 2.5, 3.0, 3.5, 4.0, 5.0, 6.0, 7.0, 8.0, 9.0, 10.0, 11, 12, 13, 14, 15, 16, 17, 18, 19, 20	2016; 2016; 2017–2022	Once; once; thrice per month
AL-S	0.1, 0.2, 0.3, 0.4, 0.5, 0.6, 0.7, 0.8, 0.9, 1.0, 1.1, 1.2, 1.3, 1.4, 2.1, 2.2, 2.3, 2.4, 2.5, 2.6, 2.7, 2.8	0.2, 0.3, 0.4, 0.5, 0.6, 0.7, 0.8, 0.9, 1.1, 1.4, 1.5, 1.7, 2.0, 2.2, 2.4, 2.6, 2.8, 2.9, 3.1, 3.4, 3.6, 4.0, 4.1, 4.5, 4.8, 5.5, 6.0, 7.0, 7.5	0.0, 0.2, 0.5, 1.0, 1.5, 2.0, 2.5, 3.0, 3.5, 4.0, 5.0, 6.0, 7.0, 8.0, 9.0, 10.0, 11, 12, 13, 14, 15, 16, 17, 18, 19, 20	2016; 2016; 2017–2022	Once; once; thrice per month
GL-U	0.1, 0.2, 0.3, 0.4, 0.5, 0.6, 0.7, 0.8, 0.9, 1.0, 1.1, 1.4, 1.5, 1.6, 1.7, 1.8, 1.9, 2.0, 2.1, 2.2, 2.3, 2.4, 2.5, 2.6, 2.7, 2.8, 2.9, 3.0, 3.1, 3.4, 3.5, 3.6	0.1, 0.2, 0.3, 0.4, 0.5, 0.6, 0.7, 0.8, 0.9, 1.0, 1.1, 1.3, 1.4, 1.5, 1.6, 1.7, 1.8, 1.9, 2.0, 2.7, 2.8, 2.9, 3.0, 3.1	0.0, 0.2, 0.5, 1.0, 1.5, 2.0, 2.5, 3.0, 3.5, 4.0, 5.0, 6.0, 7.0, 8.0, 9.0, 10.0, 11, 12, 13, 14, 15, 16, 17, 18, 19, 20	2016; 2016; 2017–2022	Once; once; thrice per month
GL-S	0.1, 0.2, 0.3, 0.4, 0.5, 0.6, 0.7, 0.8, 0.9, 1.0, 1.2, 1.3, 1.4, 1.5, 2.0, 2.1, 2.2, 2.4, 2.5, 2.6, 2.7, 2.8	0.1, 0.2, 0.3, 0.8, 2.0, 2.4, 2.7, 3.6, 4.2, 4.7, 5.6, 8.4	0.0, 0.2, 0.5, 1.0, 1.5, 2.0, 2.5, 3.0, 3.5, 4.0, 5.0, 6.0, 7.0, 8.0, 9.0, 10.0, 11, 12, 13, 14, 15, 16, 17, 18, 19, 20	2016; 2016; 2017–2022	Once; once; thrice per month
MH-U	0.1, 0.2, 0.3, 0.4, 0.5, 0.6, 0.7, 0.8, 0.9, 1.0, 1.1, 1.4, 1.5, 1.6, 1.7, 1.8, 1.9, 2.0, 2.1, 2.2, 2.3, 2.4, 2.5, 2.6, 2.7, 2.8, 2.9, 3.0, 3.1, 3.4, 3.5, 3.6	0.1, 0.2, 0.3, 0.4, 0.5, 0.6, 0.7, 0.8, 0.9, 1.0, 1.1, 1.3, 1.4, 1.5, 1.6, 1.7, 1.8, 1.9, 2.0, 2.7, 2.8, 2.9, 3.0, 3.1	0.0, 0.2, 0.5, 1.0, 1.5, 2.0, 2.5, 3.0, 3.5, 4.0, 5.0, 6.0, 7.0, 8.0, 9.0, 10.0, 11, 12, 13, 14, 15, 16, 17, 18, 19, 20	2016; 2016; 2017–2022	Once; once; thrice per month
MH-S	0.1, 0.2, 0.3, 0.4, 0.5, 0.6, 0.7, 0.8, 0.9, 1.0, 1.1, 1.2, 1.3, 1.4, 1.5, 1.6, 1.7, 1.8, 1.9, 2.0	0.1, 0.2, 0.3, 0.4, 0.5, 0.6, 0.7, 0.8, 0.9, 1.0, 1.1, 1.2, 1.3, 1.4, 1.5, 1.6, 1.7, 1.8, 1.9, 2.0, 2.3, 3.6	0.0, 0.2, 0.5, 1.0, 1.5, 2.0, 2.5, 3.0, 3.5, 4.0, 5.0, 6.0, 7.0, 8.0, 9.0, 10.0, 11, 12, 13, 14, 15, 16, 17, 18, 19, 20	2016; 2016; 2017–2022	Once; once; thrice per month

Notes: soil nutrients and SMC were observed once in 2016, and soil temperatures were observed thrice monthly in 2017–2022.

peratures showed an increasing trend of 0.01–0.69 °C yr^{-1} at depths of 0.5–20 m from 2017 to 2022. The increase rate was the largest at AL-U (rate of 0.03–0.69 °C yr^{-1}), whereas it was the lowest at AL-S and GL-S (rates of 0.01–0.37 °C yr^{-1}) (Figs. 4a–g and 5a–g).

3.2 Changes in MAGT values at the permafrost table ($MAGT_{PT}$) and D_{ZAA} ($MAGT_{DZAA}$)

MAGT values at the permafrost table ($MAGT_{PT}$) and at the D_{ZAA} ($MAGT_{DZAA}$) can truly reflect the changing characteristics of permafrost thermal regimes. Therefore, in this section, we have chosen $MAGT_{PT}$ and $MAGT_{DZAA}$ to briefly analyze changes in ground thermal regimes. When the temperature probe was missing at the actual depth of the permafrost table or the D_{ZAA}, $MAGT_{PT}$ and $MAGT_{DZAA}$ were derived from the interpolation of adjacent ground temperatures.

At the eight monitored sites, the burial depths of the permafrost table ranged between 1.5 and 4.5 m, while the depth of the D_{ZAA} ranged between 10 and 16 m. From 2017 to 2022, except at the GL-U, MH-U, and MH-S sites,

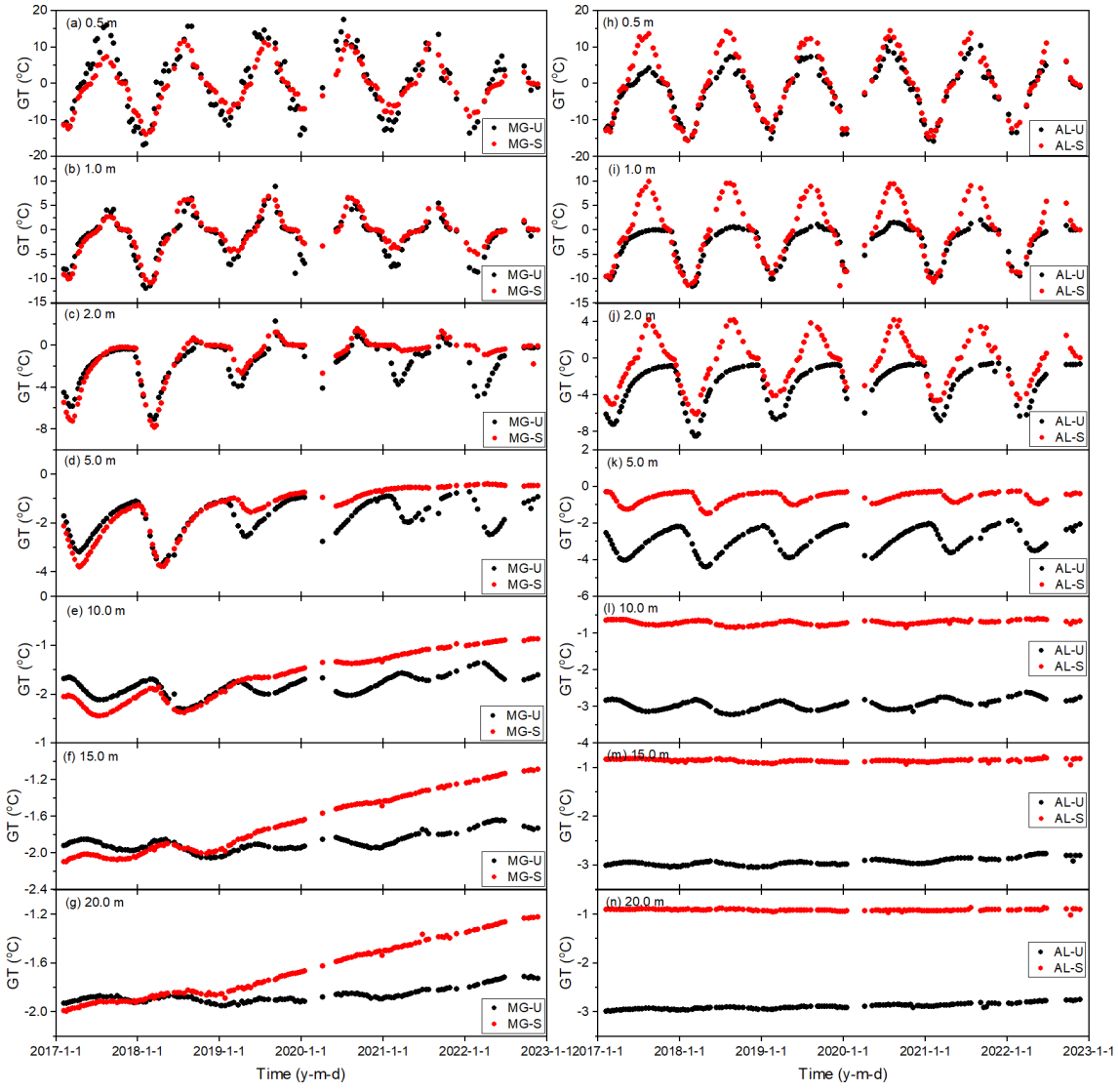

Figure 4. Variability in the ground temperature at depths of 0–20 m at Xing'an larch forest sites in Mangui (MG) and Alongshan (AL) on the western flank of the northern Da Xing'anling Mountains in Northeast China during the period from 2017 to 2022. Note that U denotes the unburned site, S denotes the severely burned site, and GT denotes ground temperature. Panels **(a)** to **(g)** show the changes in the ground temperature in Mangui (MG) 2 to 7 years after fire; panels **(h)** to **(n)** present the changes in the ground temperature in Alongshan (AL) 8 to 13 years after fire.

Table 3. Mean annual ground temperatures (MAGTs) at each of the seven measured depths at unburned and severely burned sites in the four areas on the western flank of the northern Da Xing'anling Mountains in Northeast China during the period from 2017 to 2022.

Depth (m)	0.5		1.0		2.0		5.0		10		15		20	
Fire severity	U	S	U	S	U	S	U	S	U	S	U	S	U	S
MG	0.2	−0.6	−1.5	−0.8	−1.6	−1.1	−1.7	−1.4	−1.8	−1.6	−1.9	−1.7	−1.9	−1.7
AL	−2.2	−0.3	−2.8	−0.5	−2.9	−0.6	−2.9	−0.6	−2.9	−0.7	−2.9	−0.9	−2.9	−0.9
GL	−2.7	0.5	−2.9	0.1	−3.1	−0.3	−3.1	−0.4	−2.8	−0.5	−2.6	−0.5	−2.5	−0.6
MH	−2.7	0.2	−2.9	−0.2	−3.1	−0.5	−3.1	−0.6	−2.8	−0.5	−2.6	−0.5	−2.5	−0.5

Notes: U denotes unburned sites, whereas S denotes severely burned sites.

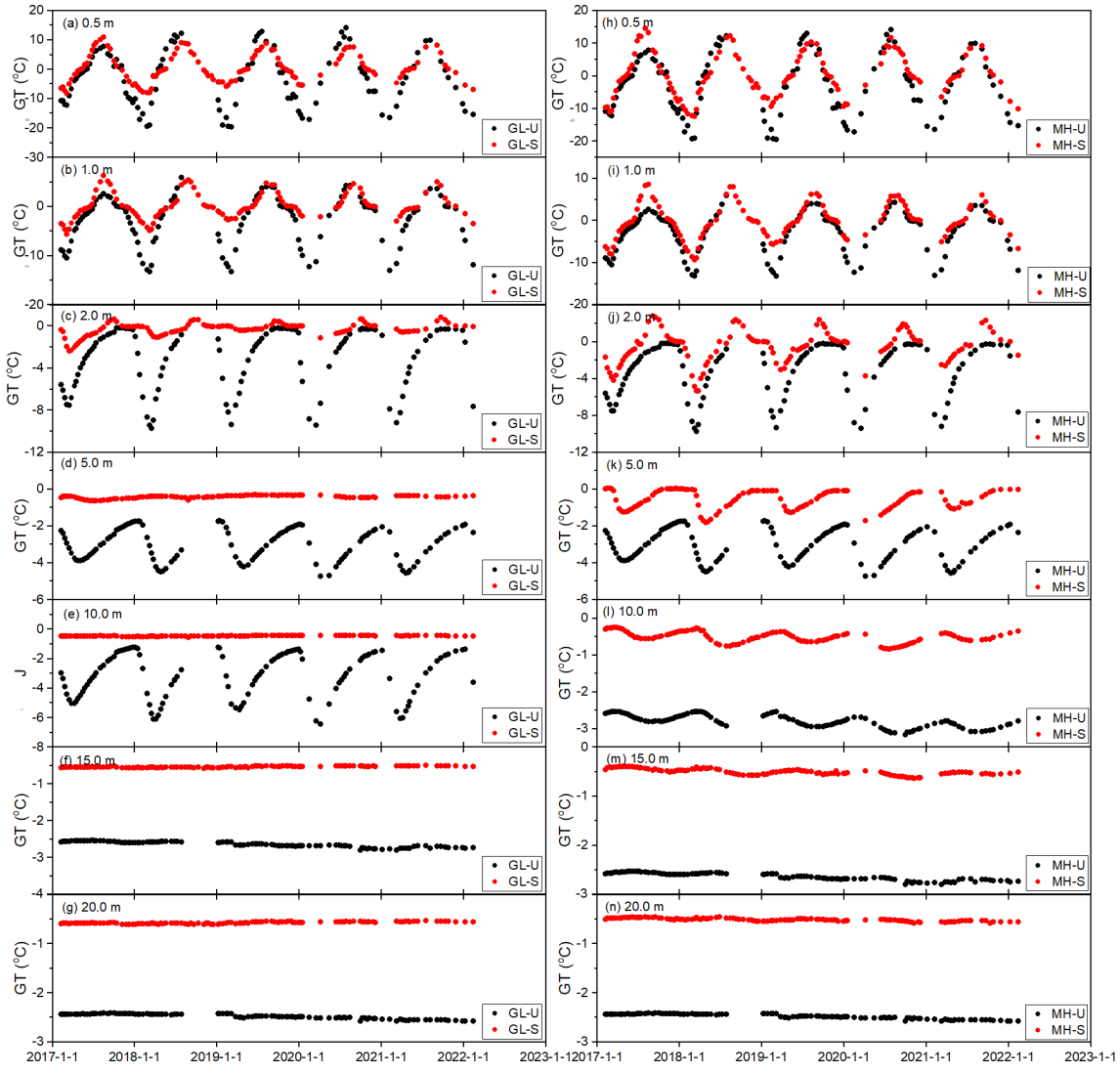

Figure 5. Variations in the ground temperature at depths of 0–20 m at shrub wetland sites in Gulian (GL) and Mo'he (MH) on the western flank of the northern Da Xing'anling Mountains in Northeast China during the period from 2017 to 2022. Note that U denotes the unburned site, S denotes the severely burned site, and GT denotes ground temperature. Panels **(a)** to **(g)** show changes in the ground temperature in GL 15–20 years after fire; panels **(h)** to **(n)** present changes in the ground temperature in MH 30–35 years after fire.

$MAGT_{PT}$ and $MAGT_{DZAA}$ decreased gradually (−0.02 to −0.06 °C yr^{-1}), whereas they increased at rates of 0.01–0.54 °C yr^{-1} at the other sites (Fig. 6). The ground warming rates of $MAGT_{PT}$ and $MAGT_{DAZZ}$ were highest at the MG-S site (both 0.54 °C yr^{-1}), whereas they were lowest at the GL-S site (0.10 and 0.01 °C yr^{-1}, respectively) (Fig. 6a and b). From 2017 to 2022, the highest differences in the $MAGT_{PT}$ and $MAGT_{DAZZ}$ were 2.6 and 1.3 °C at the MG-S site, respectively, whereas the lowest differences were 0.2 and 0.1 °C at MH-S and AL-S sites, respectively (Fig. 6a, d, and h).

3.3 Active layer thickness (ALT) data

ALT, defined as the annual maximum depth of seasonal thaw penetration, was determined according to the deepest position of the 0 °C isotherms in a year. Although some data were missing, the change trends in ALT were still obvious (Fig. 7).

ALT was between 1.0 and 5.2 m at the eight sites from 2017 to 2022. The maximum average ALT value was 4.5 m at MH-U, whereas the minimum average ALT value was 1.6 m at AL-U. Compared with the other seven sites, MH-S had the largest ALT, with the maximum ALT at 5.2 m in 2017. From 2017 and 2022, ALT decreased at a rate of 36.5 cm yr^{-1} at the MH-S site, whereas it increased at rates of 0.1–20.5 cm yr^{-1} at the other sites. The increase rate of ALT at MG-S was the fastest, where it was the slowest at AL-S (Fig. 8).

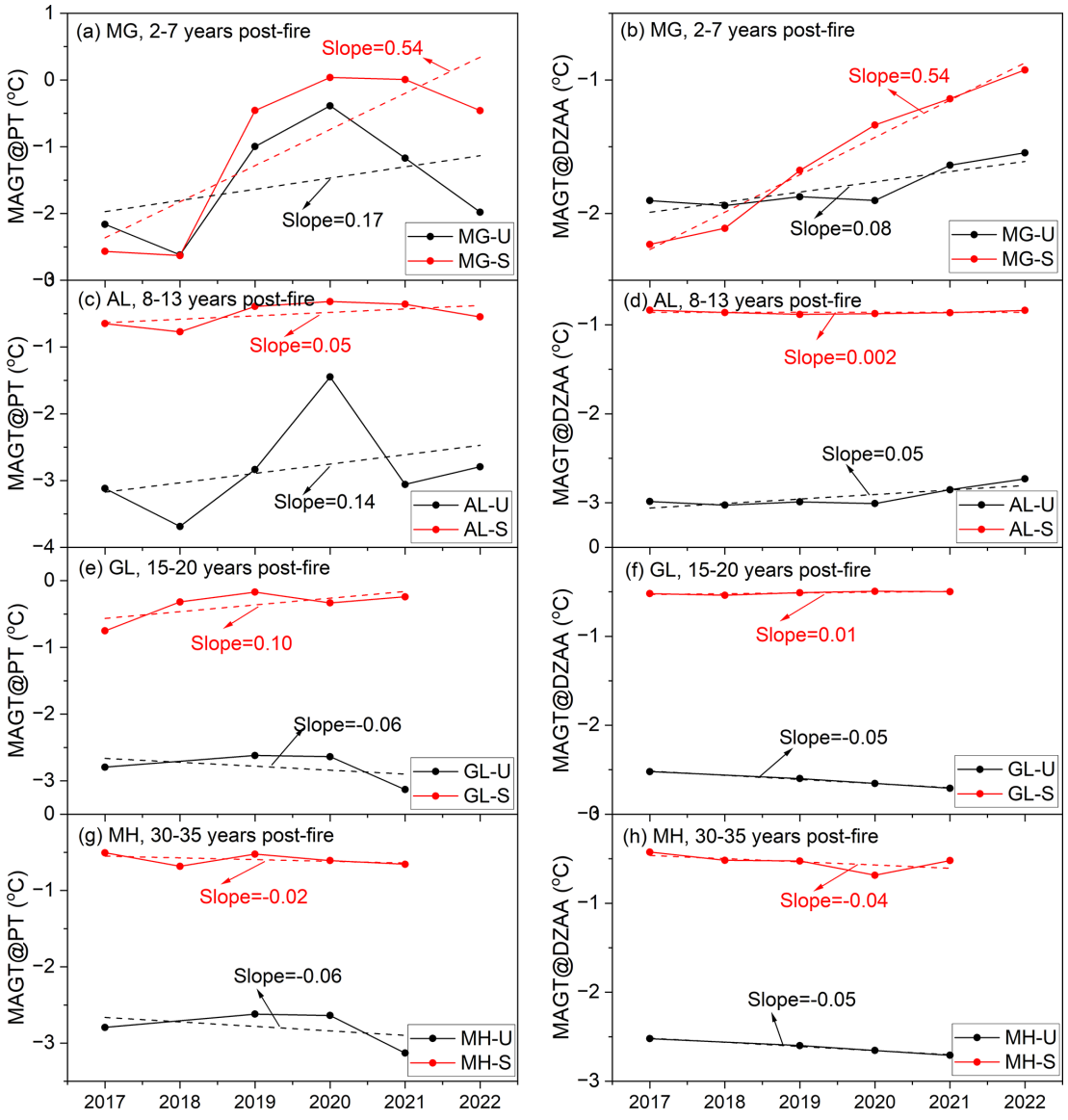

Figure 6. Variations in the mean annual ground temperature at the permafrost table ($MAGT_{PT}$) and the depth of zero annual amplitude (D_{ZAA}) ($MAGT_{DZAA}$) at eight sites in the four study areas (Mangui – MG; Alongshan – AL; Gulian – GL; and Mo'he – MH) on the western flank of the northern Da Xing'anling Mountains in Northeast China during 2017–2022. Note that U denotes unburned sites, whereas S denotes severely burned sites.

3.4 Variations in the gravimetric soil moisture content (SMC)

At the MG-U and AL-U sites, the SMC decreased with increasing depth, especially in the active layer and near-surface permafrost or in the vicinity of the permafrost table (Fig. 9). For example, at AL-U, the SMC decreased at a rate of 8.6 % m^{-1}, and the average SMC was 108.2 ± 11.7 % at depths of 0–9.4 m (Fig. 9b). At the depths (0–3 m) with a higher SMC, the soil contains massive ice crystals and a large amount of segregated ice, with ice lenses of 0.1–5.0 cm in thickness. For example, at GL-U, the SMC was higher at the junction of the bottom of the active layer and the upper layer of transient permafrost (depth of 1–2 m) due to a large amount of segregated ice (0.2–5.0 cm thick) immediately under the permafrost table. At the MG-S, AL-S, GL-S, and MH-S sites, changes in SMC were inconspicuous, only at depths of 0–0.5 m, with a slight decreasing trend. At depths of 0.5–9.4 m, differences in the SMC were minor (Fig. 9). At MG-S, the SMC fluctuated between 11.7 % and 63.2 % at depths of 0.6–7.6 m, with an average SMC of 27.5 ± 3.2 % (Fig. 9a). At the AL-S, GL-S, and MH-S sites, the SMC fluctuated between 4.7 % and 26.6 % at depths of 0.6–8.4 m, with an average SMC of 17.1 %–21.1 %.

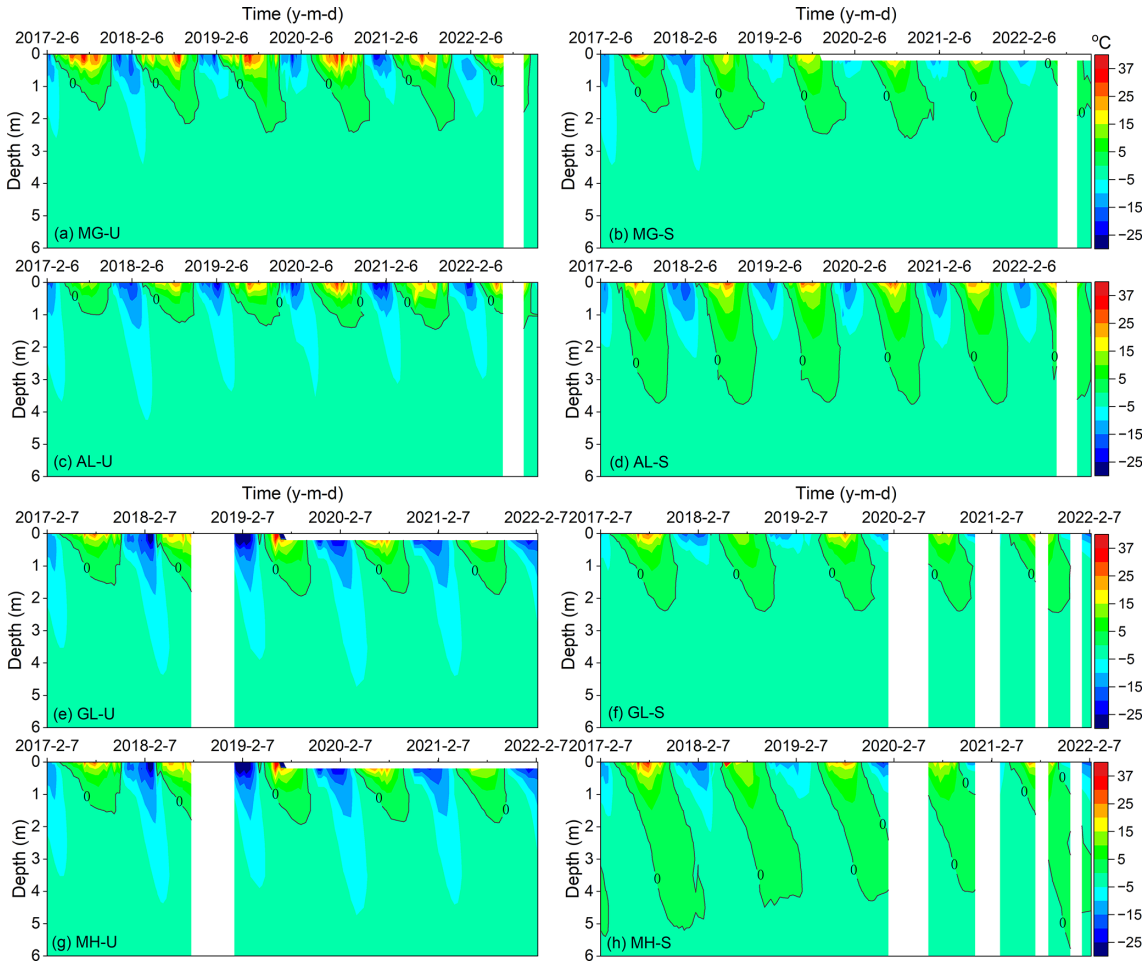

Figure 7. Variability in the ground temperature isotherms at eight sites in Mangui (MG), Alongshan (AL), Gulian (GL), and Mo'he (MH) on the western flank of the northern Da Xing'anling Mountains in Northeast China during 2017–2022. Note that U denotes unburned sites, as in panels **(a)** (site MG-U), **(c)** (site AL-U), **(e)** (site GL-U), and **(g)** (site MH-U), whereas S denotes severely burned sites, as in panels **(b)** (site MG-S), **(d)** (site AL-S), **(f)** (site GL-S), and **(h)** (site MH-S).

3.5 Variations in soil nutrients

The SOC and TN contents decreased with increasing depth. Large amounts of SOC and TN were stored in the active layer (0–1.3 m), especially in the soil organic layer (0–0.5 m) (Fig. 10a–n). The change trends in SOC and TN were consistent. For example, at MG-U, at depths of 0–1.3 m, average SOC and TN values were 140.5 ± 26.9 and $5.9 \pm 0.9\ g\ kg^{-1}$, respectively; at depths of 1.3–2.5 m, changes in SOC and TN were relatively smooth, fluctuating between 2.0–13.3 and 0.9–1.5 $g\ kg^{-1}$, with averages of 5.4 ± 1.1 and $1.2 \pm 0.1\ g\ kg^{-1}$, respectively (Fig. 10a and b).

TP contents decreased up to a depth of 1.0 m, and changes in TP were minor at depths of 1.0–5.3 m (Fig. 10c, g, k, and o). For example, at MG-S, TP decreased at a rate of $0.56\ g\ kg^{-1}\ m^{-1}$ at depths of 0–1.0 m, with an average of $0.7 \pm 0.1\ g\ kg^{-1}$ (Fig. 10c); TP fluctuated between 0.4 and $0.7\ g\ kg^{-1}$ at depths of 1.1–2.6 m, with an average of $0.6 \pm 0.01\ g\ kg^{-1}$. The change trends in TK were the opposite of those seen for TP: the TK content increased downwards (Fig. 10d, h, l, and p). The TK content values were all below $41.8\ g\ kg^{-1}$. For example, at MG-U, TK increased at a rate of $14.1\ g\ kg^{-1}\ m^{-1}$, while TP decreased at a rate of $0.5\ g\ kg^{-1}\ m^{-1}$ (Fig. 10c and d).

4 Data availability

The dataset discussed in this work can be freely downloaded from the National Tibetan Plateau/Third Pole Environment Data Center: https://doi.org/10.11888/Cryos.tpdc.300933 (Li and Jin, 2024). It has been classified into three categories: ground temperature (at MG-U, MG-S, AL-U, AL-S, GL-U, GL-S, MH-U, and MH-S), soil moisture content (SMC), and soil nutrient content (SOC, TN, TP, and TK).

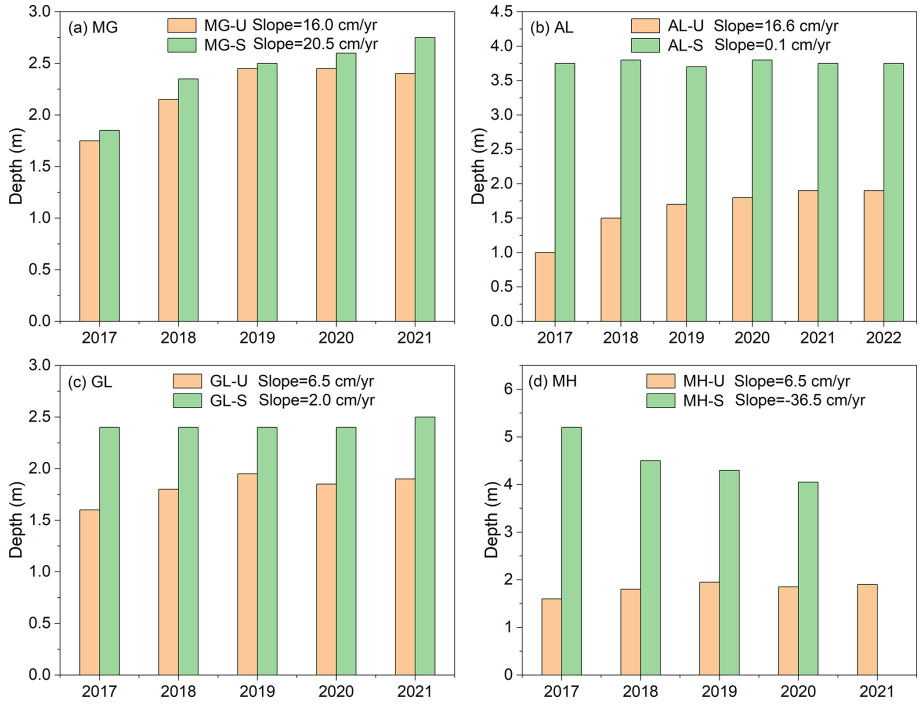

Figure 8. Variation characteristics of the active layer thickness (ALT) at eight sites in the four study areas in Mangui (MG), Alongshan (AL), Gulian (GL), and Mo'he (MH) on the western flank of the northern Da Xing'anling Mountains in Northeast China during 2017–2022. Note that U denotes the unburned site, whereas S denotes the severely burned site.

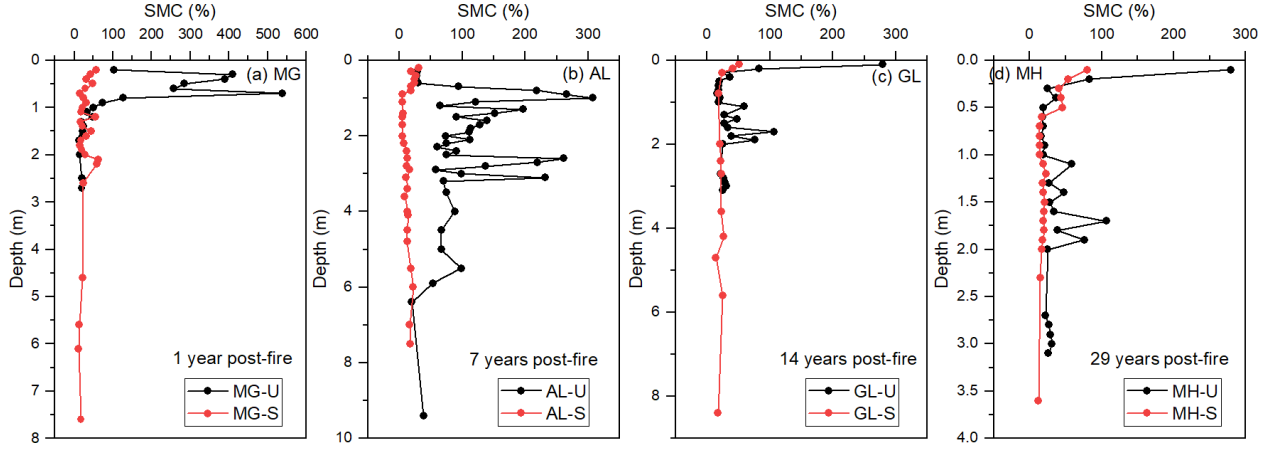

Figure 9. Variations in the gravimetrically based soil moisture content (SMC) with different fire severity levels at eight sites in Mangui (MG), Alongshan (AL), Gulian (GL), and Mo'he (MH) on the western flank of the northern Da Xing'anling Mountains in Northeast China in 2016. Note that U denotes unburned, whereas S denotes severely burned.

5 Conclusions

The Da Xing'anling Mountains in Northeast China are located on the southern margin of the eastern Asia permafrost zone and boreal forest belt. It is an area where fires occur frequently, and the thermal state of permafrost in this region is sensitive to fire disturbances. To study fire effects on the permafrost environment, a monitoring network has been established in Northeast China since 2016. Therefore, a long-term ground hydrothermal regime and soil nutrient field dataset has been obtained. This dataset fills a gap in a monitoring study of fire effects on the permafrost environment in the hemiboreal forest zone in Northeast China. These data include ground temperatures at depths of 0–20 m; SMC at depths of 0–9.4 m; and SOC, TN, TP, and TK contents at depths of 0–3.6 m. The data were collected at eight sites in four burned areas (MG, Mangui; AL, Alongshan; GL, Gu-

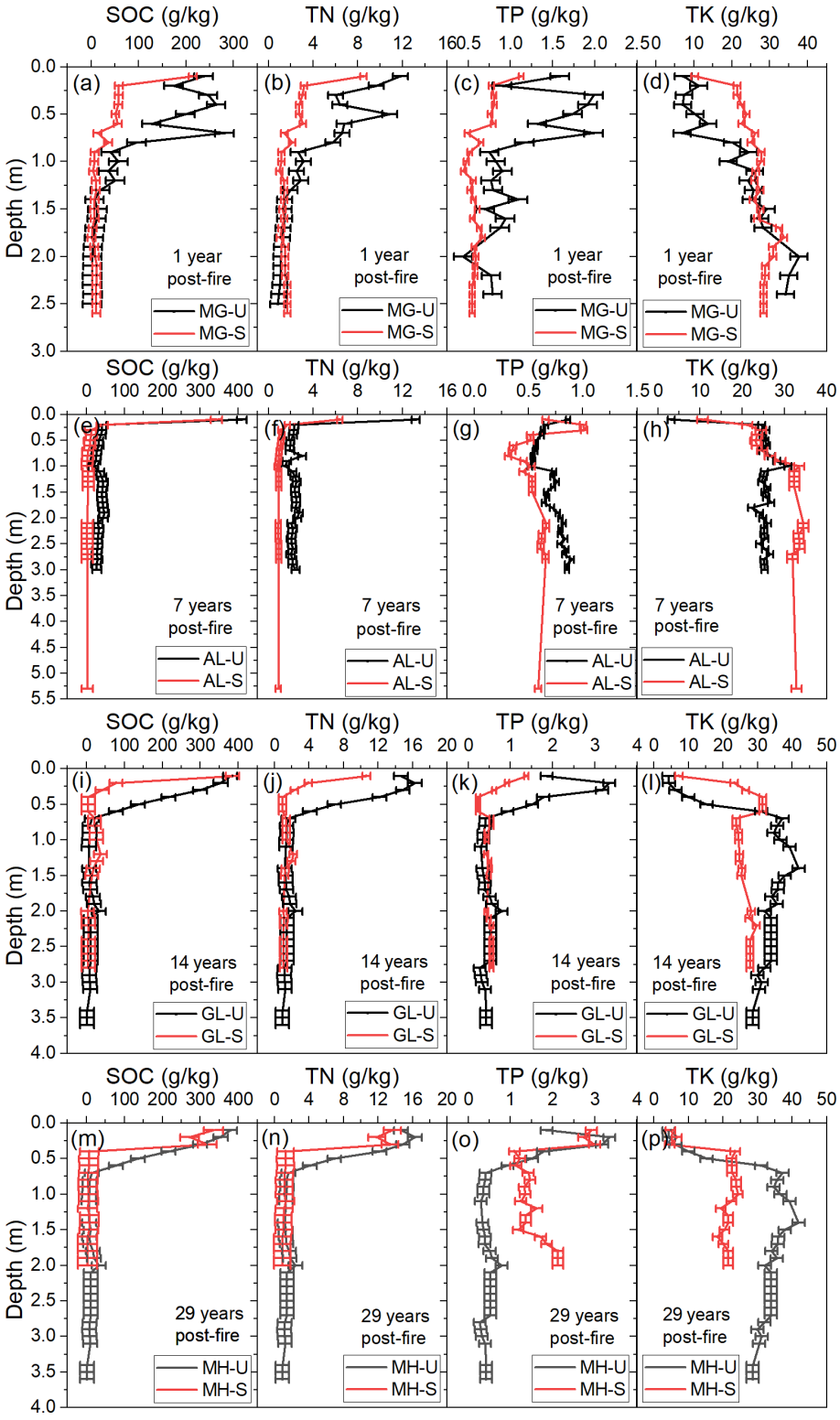

Figure 10. Variations in soil nutrients at eight sites in Mangui (MG, **a**–**d**), Alongshan (AL, **e**–**h**), Gulian (GL, **i**–**l**), and Mo'he (MH, **m**–**p**) on the western flank of the northern Da Xing'anling Mountains in Northeast China in 2016. Note that U denotes unburned, S denotes severely burned, SOC denotes soil organic carbon, TN denotes total nitrogen, TP denotes total phosphorus, and TK denotes total potassium.

lian; and MH, Mo'he) with two categories of fire severity (severely burned and unburned) from 2016 to 2022.

Long-term monitoring data in the northern Da Xing'anling Mountains in Northeast China have shown permafrost degradation due to climate change and frequent forest fire disturbances. This is evidenced by an increasing ground temperature, a thickening active layer, and evidently changing SMC and soil nutrient contents. The 6-year-long dataset presented in this study comprises a high-quality time series with only a few missing data. This valuable and hard-won dataset of forest fires and permafrost is worth maintaining and improving in the future. This work provides important basic data for the protection of the Xing'an (ecosystem-dominated) permafrost and, herewith, boreal permafrost ecosystems. Furthermore, it is useful for obtaining a more accurate prediction of fire-induced permafrost changes and for more accurate estimation and better management of soil carbon stocks. It also provides important information for carbon neutralization and carbon peak control initiatives as well as the assessment of infrastructure safety under fire threats.

Author contributions. XL and HJ designed and conducted this research. XL compiled the dataset, performed the data analysis, and wrote the manuscript. RH, HW, XC, RŞ, and ZT participated in the fieldwork. HJ, QF, QW, DL, and RŞ improved the manuscript text. XL prepared the manuscript with contributions from all co-authors.

Competing interests. The contact author has declared that none of the authors has any competing interests.

Disclaimer. Publisher's note: Copernicus Publications remains neutral with regard to jurisdictional claims made in the text, published maps, institutional affiliations, or any other geographical representation in this paper. While Copernicus Publications makes every effort to include appropriate place names, the final responsibility lies with the authors.

Acknowledgements. The authors would like to thank all of the scientists and students who participated in the fieldwork. We wish to acknowledge the two anonymous reviewers and the editor for their thorough reviews and insightful comments that improved the paper. We also are grateful to Xin Li for his encouragement, guidelines, and review of the proposal for writing up this paper and preparing the datasets.

Financial support. This research has been supported by the National Natural Science Foundation of China (grant nos. 42471166, 32241032, and 42101408); the program of the Key Laboratory of Cryospheric Science and Frozen Soil Engineering, CAS (grant no. CSFSE-ZQ-2407); the Heilongjiang Excellent Youth Fund (grant no. YQ2022D002); and the Fundamental Research Fund for the Central Universities (grant nos. 2572023CT01 and 2572021GT08). Raul-David Şerban received funding from the Autonomous Province of Bozen/Bolzano's Department for Innovation, Research and University (grant no. 13585/2023).

Review statement. This paper was edited by Sander Veraverbeke and reviewed by two anonymous referees.

References

Biskaborn, B. K., Smith, S. L., Noetzli, J., Matthes, H., Vieira, G., Streletskiy, D. A., Schoeneich, P., Romanovsky, V. E., Lewkowicz, A. G., Abramov, A., Allard, M., Boike, J., Cable, W. L., Christiansen, H. H., Delaloye, R., Diekmann, B., Drozdov, D., Etzelmuller, B., Grosse, G., Guglielmin, M., Ingeman-Nielsen, T., Isaksen, K., Ishikawa, M., Johansson, M., Johannsson, H., Joo, A., Kaverin, D., Kholodov, A., Konstantinov, P., Kroger, T., Lambiel, C., Lanckman, J. P., Luo, D., Malkova, G., Meiklejohn, I., Moskalenko, N., Oliva, M., Phillips, M., Ramos, M., Sannel, A. B. K., Sergeev, D., Seybold, C., Skryabin, P., Vasiliev, A., Wu, Q., Yoshikawa, K., Zheleznyak, M., and Lantuit, H.: Permafrost is warming at a global scale, Nat. Commun., 10, 264, https://doi.org/10.1038/s41467-018-08240-4, 2019.

Boyd, M. A., Walker, X. J., Barnes, J., Celis, G., Goetz, S. J., Johnstone, J. F., Link, N. T., Melvin, A. M., Saperstein, L., Schuur, E. A. G., and Mack, M. C.: Decadal impacts of wildfire fuel reduction treatments on ecosystem characteristics and fire behavior in Alaskan boreal forests, Forest Ecol. Manage., 546, 121347, https://doi.org/10.1016/j.foreco.2023.121347, 2023.

Brown, D. R. N., Jorgenson, M. T., Douglas, T. A., Romanovsky, V. E., Kielland, K., Hiemstra, C., Euskirchen, E. S., and Ruess, R. W.: Interactive effects of wildfire and climate on permafrost degradation in Alaskan lowland forests, J. Geophys. Res.-Biogeo., 120, 1619–1637, https://doi.org/10.1002/2015jg003033, 2015.

Certini, G.; Effects of fire on properties of forest soils: A review, Oecologia, 143, 1–10, 2005.

Chang, X., Jin, H., He, R., Zhang, Y., Li, X., Jin, X., and Li, G.: Permafrost changes in the northwestern Da Xing'anling Mountains, Northeast China, in the past decade, Earth Syst. Sci. Data, 14, 3947–3959, https://doi.org/10.5194/essd-14-3947-2022, 2022.

Chang, X., Jin, H., Zhang, Y., Li, X., He, R., Li, Y., Lü, L., and Wang, H.: Permafrost thermal dynamics at a local scale in northern Da Xing'anling Mountains, Environ. Res. Lett., 19, 064014, https://doi.org/10.1088/1748-9326/ad42b6, 2024.

Chen, X., Kang, S., Hu, Y., and Yang, J.: Temporal and spatial analysis of vegetation fire activity in the circum-Arctic during 2001–2020, Res. Cold Arid Reg., 15, 48–56, https://doi.org/10.1016/j.rcar.2023.03.002, 2023.

Chen, Y., Kelly, R., Genet, H., Lara, M. J., Chipman, M. L., McGuire, A. D., and Hu, F. S.: Resilience and sensitivity of ecosystem carbon stocks to fire-regime change in Alaskan tundra, Sci. Total Environ., 806, 151482, https://doi.org/10.1016/j.scitotenv.2021.151482, 2022.

Cocke, A. E., Fulé, P. Z., and Crouse, J. E.: Comparison of burn severity assessments using Differenced Normalized Burn Ratio and ground data, Int. J. Wildland Fire, 14, 189–198, 2005.

Cunningham, C. X., Williamson, G. J., and Bowman, D. M.: Increasing frequency and intensity of the most extreme wildfires on Earth, Nat. Ecol. Evol., 8, 1420–1425, https://doi.org/10.1038/s41559-024-02452-2, 2024.

Dieleman, C. M., Day, N. J., Holloway, J. E., Baltzer, J., Douglas, T. A., and Turetsky, M. R.: Carbon and nitrogen cycling dynamics following permafrost thaw in the Northwest Territories, Canada, Sci. Total Environ., 845, 157288, https://doi.org/10.1016/j.scitotenv.2022.157288, 2022.

Escuin, S., Navarro, R., and Fernandez, P.: Fire severity assessment by using NBR (normalized Burn ratio) and NDVI (normalized difference vegetation index) derived from Landsat TM/ETM images, Int. J. Remote Sens., 29, 1053–1073, 2008.

Fultz, L. M., Moore-Kucera, J., Dathe, J., Davinic, M., Perry, G., Wester, D., Schwilk, D. W., and Rideout-Hanzak, S.: Forest wildfire and grassland prescribed fire effects on soil biogeochemical processes and microbial communities: Two case studies in the semi-arid Southwest, Appl. Soil Ecol., 99, 118–128, https://doi.org/10.1016/j.apsoil.2015.10.023, 2016.

Genet, H., McGuire, A. D., Barrett, K., Breen, A., Euskirchen, E. S., Johnstone, J. F., Kasischke, E. S., Melvin, A. M., Bennett, A., Mack, M. C., Rupp, T. S., Schuur, A. E. G., Turetsky, M. R., and Yuan, F.: Modeling the effects of fire severity and climate warming on active layer thickness and soil carbon storage of black spruce forests across the landscape in interior Alaska, Environ. Res. Lett., 8, 045016, https://doi.org/10.1088/1748-9326/8/4/045016, 2013.

Gu, H., Jin, J., Cheng, X., Wang, E., Zhou, Y., and Chai, Y.: The long-term impacts on chemical properties of Larix gmelini forest on the northern slope of greater Hinggan Mountains from a forest fire of varying fire intensity, J. Nat. Resour., 25, 1114–1121, 2010 (in Chinese).

Holloway, J. E., Lewkowicz, A. G., Douglas, T. A., Li, X., Turetsky, M. R., Baltzer, J. L., and Jin, H.: Impact of wildfire on permafrost landscapes: a review of recent advances and future prospects, Permafrost Periglac., 31, 371–382, 2020.

Hugelius, G., Strauss, J., Zubrzycki, S., Harden, J. W., Schuur, E. A. G., Ping, C.-L., Schirrmeister, L., Grosse, G., Michaelson, G. J., Koven, C. D., O'Donnell, J. A., Elberling, B., Mishra, U., Camill, P., Yu, Z., Palmtag, J., and Kuhry, P.: Estimated stocks of circumpolar permafrost carbon with quantified uncertainty ranges and identified data gaps, Biogeosciences, 11, 6573–6593, https://doi.org/10.5194/bg-11-6573-2014, 2014.

Jin, H., Li, S., Cheng, G., Wang, S., and Li, X.: Permafrost and climatic change in China, Global Planet. Change, 26, 387–404, https://doi.org/10.1016/S0921-8181(00)00051-5, 2000.

Jin, H., Yu, Q., Lü, L., Guo, D., He, R., Yu, S., Sun, G., and Li, Y.: Degradation of permafrost in the Xing'anling Mountains, northeastern China, Permafrost Periglac., 18, 245–258, https://doi.org/10.1002/ppp.589, 2007.

Jin, H., Wu, Q., and Romanovsky, V. E.: Editorial: Impacts from degrading permafrost, Adv. Clim. Change Res., 12, 1–5, https://doi.org/10.1016/j.accre.2021.01.007, 2021.

Jin, H., Huang, Y., Bense, V. F., Ma, Q., Marchenko, S. S., Shepelev, V. V., Hu, Y., Liang, S., Spektor, V. V., Jin, X., Li, X., and Li X.: Permafrost degradation and its hydrogeological impacts, Water, 14, 372, https://doi.org/10.3390/w14030372, 2022.

Jin, H., Yang, D., Makarieva, O., and Tang, L.: Changes in permafrost and snow cover in the Boreal and Arctic zones (BAZ) and their impacts, Adv. Clim. Change Res., 14, 157–163, https://doi.org/10.1016/j.accre.2023.04.002, 2023.

Johnstone, J. F., Chapin Iii, F. S., Foote, J., Kemmett, S., Price, K., and Viereck, L.: Decadal observations of tree regeneration following fire in boreal forests, Can. J. Forest Res., 34, 267–273, https://doi.org/10.1139/x03-183, 2004.

Johnstone, J. F., Hollingsworth, T. N., Chapin Iii, F. S., and Mack, M. C.: Changes in fire regime break the legacy lock on successional trajectories in Alaskan boreal forest, Glob. Change Biol., 16, 1281–1295, https://doi.org/10.1111/j.1365-2486.2009.02051.x, 2010.

Jones, B. M., Grosse, G., Arp, C. D., Miller, E., Liu, L., Hayes, D. J., and Larsen, C. F.: Recent Arctic tundra fire initiates widespread thermokarst development, Sci. Rep., 5, 15865, https://doi.org/10.1038/srep15865, 2015.

Jorgenson, M. T., Harden, J., Kanevskiy, M., O'Donnell, J., Wickland, K., Ewing, S., Manies, K., Zhuang, Q. L., Shur, Y., Striegl, R., and Koch, J.: Reorganization of vegetation, hydrology and soil carbon after permafrost degradation across heterogeneous boreal landscapes, Environ. Res. Lett., 8, 035017, https://doi.org/10.1088/1748-9326/8/3/035017, 2013.

Key, C. H. and Benson, N. C.: Landscape assessment (LA), Sampling and analysis methods, edited by: Lutes, D. C., Keane, R. E., Caratti, J. F., Key, C. H., Benson, N. C., Sutherland, S., and Gangi, L. J., FIREMON: Fire effects monitoring and inventory system. Integration of standardized field data collection techniques and sampling design with remote sensing to assess fire effects, U.S. Department of Agriculture, Forest Service, Rocky Mountain Research Station, Fort Collins, CO, LA1–LA51, Gen. Tech. Rep. RMRS-GTR-164-CD, 2006.

Kirdyanov, A. V., Saurer, M., Siegwolf, R., Knorre, A. A., Prokushkin, A. S., Churakova, O. V., Fonti, M. V., and Büntgen, U.: Long-term ecological consequences of forest fires in the continuous permafrost zone of Siberia, Environ. Res. Lett., 15, 034061, https://doi.org/10.1088/1748-9326/ab7469, 2020.

Knicker, H.: How does fire affect the nature and stability of soil organic nitrogen and carbon? A review, Biogeochemistry, 85, 91–118, 2007.

Knorr, W., Arneth, A., and Jiang, L.: Demographic controls of future global fire risk, Nat. Clim. Change, 6, 781–785, https://doi.org/10.1038/nclimate2999, 2016.

Kolka, R. K., Sturtevant, B. R., Miesel, J. R., Singh, A., Wolter, P. T., Fraver, S., DeSutter, T. M., and Townsend, P. A.: Emissions of forest floor and mineral soil carbon, nitrogen and mercury pools and relationships with fire severity for the Pagami Creek Fire in the Boreal Forest of northern Minnesota, Int. J. Wildland Fire., 26, 296–305, 2017.

Kopp, B. J., Minderlein, S., and Menzel, L.: Soil moisture dynamics in a mountainous headwater area in the discontinuous permafrost zone of northern Mongolia, Arct. Antarct. Alp. Res., 46, 459–470, 2014.

Koven, C. D., Schuur, E. A. G., Schädel, C., Bohn, T. J., Burke, E. J., Chen, G., Chen, X., Ciais, P., Grosse, G., Harden, J. W., Hayes, D. J., Hugelius, G., Jafarov, E. E., Krinner, G., Kuhry, P., Lawrence, D. M., MacDougall, A. H., Marchenko, S. S., McGuire, A. D., Natali, S. M., Nicolsky, D. J., Olefeldt, D., Peng, S., Romanovsky, V. E., Schaefer, K. M., Strauss, J., Treat, C. C., and Turetsky, M.: A simplified, data-constrained approach to estimate the permafrost carbon–climate

feedback, Philos. T. R. Soc. Lond. Ser. A-Math., 373, 20140423, https://doi.org/10.1098/rsta.2014.0423, 2015.

Li, G., Ma, W., Wang, F., Jin, H., Fedorov, A., Chen, D., Wu, G., Cao, Y., Zhou, Y., Mu, Y., Mao, Y., Zhang, J., Gao, K., Jin, X., He, R., Li, X., and Li, Y.: A newly integrated ground temperature dataset of permafrost along the China–Russia crude oil pipeline route in Northeast China, Earth Syst. Sci. Data, 14, 5093–5110, https://doi.org/10.5194/essd-14-5093-2022, 2022.

Li, X. and Jin, H.: An integrated dataset of ground hydrothermal regimes and soil nutrients monitored during 2016-2022 in burned areas in Northeast China, National Tibetan Plateau/Third Pole Environment Data Center [data set], https://doi.org/10.11888/Cryos.tpdc.300933, 2024.

Li, X., Jin, H., He, R., Huang, Y., Wang, H., Luo, D., Jin, X., Lu, L., Wang, L., Li, W., Wei, C., Chang, X., Yang, S., and Yu, S.: Effects of forest fires on the permafrost environment in the northern Da Xing'anling (Hinggan) mountains, Northeast China, Permafrost Periglac., 30, 163–177, 2019.

Li, X., Jin, H., Wang, H., Marchenko, S. S., Shan, W., Luo, D., He, R., Spektor, V., Huang, Y., Li, X., and Jia, N.: Influences of forest fires on the permafrost environment: A review, Adv. Clim. Change Res., 12, 48–65, 2021.

Li, X., Jin, H., Wang, H., Jin, X., Bense, V. F., Marchenko, S. S., He, R., Huang, Y., and Luo, D.: Effects of fire history on thermal regimes of permafrost in the northern Da Xing'anling Mountains, NE China, Geoderma, 410, 115670, https://doi.org/10.1016/j.geoderma.2021.115670, 2022a.

Li, X., Jin, H., Sun, L., Wang, H., Huang, Y., He, R., Chang, X., Yu, S. and Zang, S.: TTOP-model-based maps of permafrost distribution in Northeast China for 1961–2020, Permafrost Periglac., 33, 425–435, https://doi.org/10.1002/ppp.2157, 2022b.

Li, X., Jin, H., He, R., Wang, H., Sun, L., Luo, D., Huang, Y., Li, Y., Chang, X., Wang, L., and Wei, C.: Impact of wildfire on soil carbon and nitrogen storage and vegetation succession in the Nanweng'he National Natural Wetlands Reserve, Northeast China, Catena, 221, 106797, https://doi.org/10.1016/j.catena.2022.106797, 2023.

Liang, L., Zhou, Y., Wang, J., and Gao, X.: Changes of the permafrost environment in Great Xian Ridge after disastrous forest fire, Taking Gulian mining area as an example (in Chinese), J. Glaciol. Geocryol., 13, 17–25, https://doi.org/10.7522/j.issn.1000-0240.1991.0003, 1991.

Mack, M. C., Bret-Harte, M. S., Hollingsworth, T. N., Jandt, R. R., Schuur, E. A., Shaver, G. R., and Verbyla, D. L.: Carbon loss from an unprecedented Arctic tundra wildfire, Nature, 475, 489–492, 2011.

Mack, M. C., Walker, X. J., Johnstone, J. F., Alexander, H. D., Melvin, A. M., Jean, M., and Miller, S. N.: Carbon loss from boreal forest wildfires offset by increased dominance of deciduous trees, Science, 372, 280–283, https://doi.org/10.1126/science.abf3903, 2021.

Michaelides, R. J., Schaefer, K., Zebker, H. A., Parsekian, A., Liu, L., Chen, J. Y., Natali, S., Ludwig, S., and Schaefer, S. R.: Inference of the impact of wildfire on permafrost and active layer thickness in a discontinuous permafrost region using the remotely sensed active layer thickness (ReSALT) algorithm, Environ. Res. Lett., 14, 035007, https://doi.org/10.1088/1748-9326/aaf932, 2019.

Munkhjargal, M., Yadamsuren, G., Yamkhin, J., and Menzel, L.: The combination of wildfire and changing climate triggers permafrost degradation in the Khentii Mountains, northern Mongolia, Atmosphere, 11, 155, https://doi.org/10.3390/atmos11020155, 2020.

Neff, J. C., Harden, J. W., and Gleixner, G.: Fire effects on soil organic matter content, composition, and nutrients in boreal interior Alaska, Can. J. Forest Res., 35, 2178–2187, 2005.

Nelson, D. W., Sommers, L., Page, A. L., Miller, R. H., and Keeney, D. R.: Total carbon, organic carbon, and organic matter, in: Methods of Soil Analysis, Part 3, edited by: Sparks, D. L., Page, A. L., Helmke, P. A., and Loeppert, R. H., Soil Science Society of America, Madison, WI, USA, 539–552, https://doi.org/10.2134/agronmonogr9.2.2ed.c29, 1982.

Nossov, D. R., Jorgenson, M. T., Kielland, K., and Kanevskiy, M. Z.: Edaphic and microclimatic controls over permafrost response to fire in interior Alaska, Environ. Res. Lett., 8, 035013, https://doi.org/10.1088/1748-9326/8/3/035013, 2013.

O'Donnell, J. A., Harden, J. W., McGuire, A. D., Kanevskiy, M. Z., Jorgenson, M. T., and Xu, X.: The effect of fire and permafrost interactions on soil carbon accumulation in an upland black spruce ecosystem of interior Alaska: Implications for post-thaw carbon loss, Glob. Change Biol., 17, 1461–1474, 2011a.

O'Donnell, J. A., Harden, J. W., McGuire, A. D., and Romanovsky, V. E.: Exploring the sensitivity of soil carbon dynamics to climate change, fire disturbance and permafrost thaw in a black spruce ecosystem, Biogeosciences, 8, 1367–1382, https://doi.org/10.5194/bg-8-1367-2011, 2011b.

Petrov, M. I., Fedorov, A. N., Konstantinov, P. Y., and Argunov, R. N.: Variability of permafrost and landscape conditions following forest fires in the Central Yakutian Taiga Zone, Land, 11, 496, https://doi.org/10.3390/land11040496, 2022.

Ping, C. L., Michaelson, G. J., Kane, E. S., Packee, E. C., Stiles, C. A., Swanson, D. K., and Zaman, N. D.: Carbon stores and biogeochemical properties of soils under black spruce forest, Alaska, Soil Sci. Soc. Am. J., 74, 969–978, https://doi.org/10.2136/sssaj2009.0152, 2010.

Potter, C. and Hugny, C.: Wildfire effects on permafrost and soil moisture in spruce forests of interior Alaska, J. Forest Res., 31, 553–563, 2020.

Ramm, E., Ambus, P. L., Gschwendtner, S., Liu, C., Schloter, M., and Dannenmann, M.: Fire intensity regulates the short-term postfire response of the microbiome in Arctic tundra soil, Geoderma, 438, 116627, https://doi.org/10.1016/j.geoderma.2023.116627, 2023.

Rocha, A. V., Loranty, M. M., Higuera, P. E., Mack, M. C., Hu, F., Jones, B. M., Breen, A. L., Rastetter, E. B., Goetz, S. J., and Shaver, G. R.: The footprint of Alaskan tundra fires during the past half-century: implications for surface properties and radiative forcing. Environ. Res. Lett., 7, 044039, https://doi.org/10.1088/1748-9326/7/4/044039, 2012.

Roy, D. P., Boschetti, L., and Trigg, S. N.: Remote sensing of fire severity: assessing the performance of the normalized burn ratio, IEEE Geosci. Remote Sens. Lett., 3, 112–116, 2006.

Şerban, R. D., Şerban, M., He, R., Jin, H., Li, Y., Li, X., Wang, X., and Li, G.: 46-Year (1973–2019) permafrost landscape changes in the Hola Basin, Northeast China using machine learning and object-based classification, Remote Sens., 13, 1910, https://doi.org/10.3390/rs13101910, 2021.

Shur, Y. L. and Jorgenson, M. T.: Patterns of permafrost formation and degradation in relation to climate and ecosystems, Permafrost Periglac., 18, 7–19, 2007.

Smith, S. L., Riseborough, D. W., and Bonnaventure, P. P.: Eighteen year record of forest fire effects on ground thermal regimes and permafrost in the Central Mackenzie Valley, NWT, Canada, Permafrost Periglac., 26, 289–303, 2015.

Smith, S. L., O'Neill, H. B., Isaksen, K., Noetzli, J., and Romanovsky, V. E.: The changing thermal state of permafrost, Nat. Rev. Earth Environ., 3, 10–23, 2022.

Soil Survey Staff: Keys to Soil Taxonomy, 12th Edn., Natural Resources Conservation Service, United States Department of Agriculture, Washington D.C., ISBN 9780160923210, 2014.

Sun, L., Zhao, J., and Hu, H.: Effect of moderate fire disturbance on soil physical and chemical properties of *Betula platyphylla-Larix gmelinii* mixed forest, Sci. Silvae Sinicae, 47, 103–110, 2011 (in Chinese).

Taş, N., Prestat, E., McFarland, J. W., Wickland, K. P., Knight, R., Berhe, A. A., Jorgenson, T., Waldrop, M. P., and Jansson, J. K.: Impact of fire on active layer and permafrost microbial communities and metagenomes in an upland Alaskan boreal forest, ISME J., 8, 1904–1919, 2014.

Turetsky, M. R., Abbott, B. W., Jones, M. C., Anthony, K. W., Olefeldt, D., Schuur, E. A. G., Koven, C., McGuire, A. D., Grosse, G., Kuhry, P., Hugelius, G., Lawrence, D. M., Gibson, C., and Sannel, A. B. K.: Permafrost collapse is accelerating carbon release, Nature, 569, 32–34, 2019.

Viereck, L. A., Werdin-Pfisterer, N. R., Adams, P. C., and Yoshikawa, K.: Effect of wildfire and fireline construction on the annual depth of thaw in a black spruce permafrost forest in interior alaska: a 36-year record of recovery, in: Proceedings of the Ninth International Conference on Permafrost, edited by: Kane, D. L. and Hinkel, K. M., Fairbanks, Alaska, USA, 29 June to 3 July, Vol. 2, 1845–1850, 2008.

Wang, H., Jin, H., Che, T., Li, X., Dai, L., Qi, Y., Huang, C., He, R., Zhang, J., Yang, R., Luo, D., and Jin, X.: Influences of snow cover on the thermal regimes of Xing'an permafrost in Northeast China in 1960s–2010s, Permafrost Periglac., 35, 188–201, https://doi.org/10.1002/ppp.2223, 2024.

Westerling, A. L., Hidalgo, H. G., Cayan, D. R., and Swetnam, T. W.: Warming and earlier spring increase Western U.S. forest wildfire activity, Science, 313, 940–943, https://doi.org/10.1126/science.1128834, 2006.

Xu, W., Elberling, B., and Ambus, P. L.: Long-term summer warming reduces post-fire carbon dioxide losses in an arctic heath tundra, Agr. Forest Meteorol., 344, 109823, https://doi.org/10.1016/j.agrformet.2023.109823, 2024.

Yoshikawa, K., Bolton, W. R., Romanovsky, V. E., Fukuda, M., and Hinzman, L. D.: Impacts of wildfire on the permafrost in the boreal forests of Interior Alaska, J. Geophys. Res., 108, 8148, https://doi.org/10.1029/2001JD000438, 2003.

Zhao, K., Zhang, W., Zhou, Y., and Yang, Y.: The influence and countermeasure of forest fire on environment in Da Xing 'anling Mountains, Beijing, Science Press, ISBN 9787544518161, 1994 (in Chinese).

Zhao, L., Zou, D., Hu, G., Wu, T., Du, E., Liu, G., Xiao, Y., Li, R., Pang, Q., Qiao, Y., Wu, X., Sun, Z., Xing, Z., Sheng, Y., Zhao, Y., Shi, J., Xie, C., Wang, L., Wang, C., and Cheng, G.: A synthesis dataset of permafrost thermal state for the Qinghai–Tibet (Xizang) Plateau, China, Earth Syst. Sci. Data, 13, 4207–4218, https://doi.org/10.5194/essd-13-4207-2021, 2021.

Zhou, Y., Liang, L., and Gu, Z.: Effects of forest fire on hydrothermal regime of frozen ground, the northern part of the Da Hinggan Ling (in Chinese), J. Glaciol. Geocryol., 15, 17–26, 1993.